



# Hole quality and thermal defects in drilled CFRP by nanosecond pulsed laser

Xinyi Liu<sup>1</sup> · Sen Yang<sup>2,3</sup> · Youdong Gao<sup>1</sup> · Man Xu<sup>1</sup> · Yu Wan<sup>1</sup> · Meng Wu<sup>1</sup> · Lin Li<sup>1</sup> · Chenzhuo Wang<sup>1</sup> · Mian Zhong<sup>4</sup> · Biyi Wang<sup>5</sup> · Yong Jiang<sup>1</sup>

Received: 11 October 2023 / Accepted: 30 March 2024 / Published online: 19 April 2024  
© The Author(s), under exclusive licence to Springer-Verlag London Ltd., part of Springer Nature 2024

## Abstract

The aim of this work was to investigate the impact of nanosecond pulse laser drilling on the quality of carbon fiber reinforced polymer (CFRP). The effects of laser parameters, including laser power, scan speed, pulse width and laser frequency on micro-hole quality and the thermal damage generated during the drilling process were analyzed. 0.4 mm diameter micro-holes were drilling using a 1064 nm fiber laser, using univariate and orthogonal experimental method. The results indicate that pumping at the entrance leads to a significant increase in hole diameter and heat-affected zone (HAZ) width at both the entrance and exit, as laser power, pulse width and frequency increase, and scanning speed decrease. The width of the HAZ at the exit is dependent on whether the energy reaches the carbon fiber ablation threshold. The holes were tapered and the hole taper was closely related to the change in laser parameters at the entrance and exit of the hole. A taper of approximately 0.3 was achieved with a combination of 99 W, 50 mm/s, 13 ns and 1500 kHz. The experiments indicate that laser power and pulse width are crucial factors that affect the quality of micro-hole processing. However, nanosecond laser drilling can result in thermal damage defects, including striations, micro-cracks, delamination, voids and surface fiber ‘fish scale’ peeling.

**Keywords** Fiber laser · CFRP · Laser drilling · Thermal defects · Hole quality

## 1 Introduction

The demand for lightweight structural products has led to an increasing attention to composite materials. Carbon fiber reinforced polymer (CFRP) [1] has emerged as

a typical representative composite material due to its ability to achieve both lightweight and structure-function integration. CFRP has excellent properties, including high specific strength, low density, strong corrosion resistance, high design capability and good fatigue resistance [2]. It is widely used in aerospace, transportation, medical equipment, national defense and military products [3, 4]. Currently, CFRP products require processing such as cutting and drilling to meet people’s needs. The anisotropy of CFRP presents significant challenges for high-quality processing [5]. Traditional mechanical drilling often results in defects such as high material delamination, burrs, and cracks at the edge of the hole, causing severe tool wear and increased processing costs [6, 7].

Electrical discharge machining (EDM) [8] and ultrasonic machining [7] are inefficient methods that produce more defects in the holes [9]. Ultrasonic machining also presents a challenge in solving the resonance frequency matching problem [7]. Although abrasive water jet machining has the advantage of low thermal damage, controlling machining accuracy remains difficult, leading to defects such as high

✉ Yong Jiang  
y\_jiang@swust.edu.cn

<sup>1</sup> School of Mathematics and Physics, Southwest University of Science and Technology, Mianyang 621010, China

<sup>2</sup> Xi’an LaSiC Semiconductor Technology Co.,Ltd, Xi’an 710000, China

<sup>3</sup> Department of Microelectronics, School of Electronic and Information Engineering, Xi’an Jiaotong University, Xi’an 710049, China

<sup>4</sup> Institute of Electronic and Electrical Engineering, Civil Aviation Flight University of China, Guanghan 618307, China

<sup>5</sup> National Key Laboratory of Electromagnetic Space Security, Tianjin 300308, China

surface roughness and material delamination [10]. In addition, the hygroscopic properties of CFRP can significantly reduce its mechanical properties when subjected to abrasive water jet processing [11, 12]. Laser processing technology is a novel process that boasts high machining accuracy, high efficiency, no tool wear, non-contact, low cost and easy control [13]. This technology can effectively reduce hole defects in CFRP hole drilling by achieving thermal ablation removal of materials through the absorption of laser energy. The thermal properties of carbon fiber and matrix material differ greatly, which can result in thermal damage, particularly in the heat-affected zone (HAZ). This damage can significantly reduce the mechanical properties of the material [14, 15].

To address the above issues outlined above, Herzog et al. [16] compared the effects of pulsed Nd: YAG laser, disk and CO<sub>2</sub> lasers on the cutting quality and static strength of CFRP at different laser powers. The results showed that pulsed lasers can decrease the contact time between the laser and the material. In comparison to the other two lasers, the pulsed laser resulted in a smaller HAZ and higher static strength (1000 MPa) and bending strength (2600 MPa). Li et al. [17] investigated the hole quality and tensile strength of CFRP using fiber lasers in continuous and pulsed modes. They concluded that the pulsed laser produced better processing quality. Ramanujam et al. [18] studied the quality of the holes in CFRP materials following continuous CO<sub>2</sub> laser processing. They found that irregular micro-hole profiles appeared at the entrance and exit under all parameter conditions. Zhou et al. [19] analyzed the physical process of QCW fiber millisecond laser processing of CFRP. They identified that hole drilling involves physical processes such as thermal evaporation, melting, plasma impact, mechanical ablation, pyrolysis and carbonization. Sato et al. [20] compared the effects of N<sub>2</sub> and air assistance on the quality of CFRP processed by a 1064 nm pulsed fiber laser. The results showed that N<sub>2</sub> assistance effectively inhibits HAZ formation and increases the cutting speed. Romoli et al. [21] demonstrated that the epoxy resin has minimal absorption of the 1064 nm laser, while the carbon fibers absorb it. Therefore, under the laser irradiation of this wavelength, the HAZ is mainly formed by the heat conduction of the carbon fiber. Takahashi et al. [22] analyzed the quality of Nd: YAG laser cutting of CFRP at 1064 nm and 266 nm through theoretical simulation and experimentation. The results showed that the 1064 nm laser passes through the resin and strongly heats the carbon fiber. Tao et al. [23] investigated the bowl bottom effect of taper generated during 1064 nm drilling. They found that this effect is related to the Gaussian distribution characteristics of the laser beam during the initial taper formation stage I, the decrease in average laser fluence due to the expansion of the beam area during taper accumulation

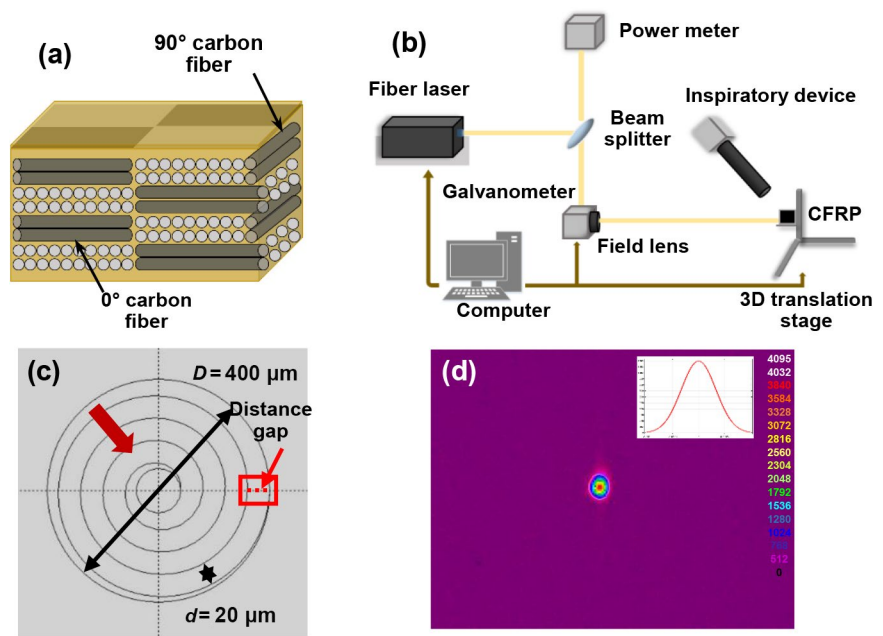
stage II, and secondary processing during bowl bottom formation stage III.

The process of laser drilling primarily removes the molten material laterally and discharges it axially along the hole depth. The choice of drilling method, in addition to the influence of laser parameter factors, also aids in reducing the recast layer and improving the geometric accuracy of laser drilling [24, 25]. Li et al. [26] investigated the effects of various scanning strategies on hole drilling, and the found that spiral scanning could significantly reduce the width of the HAZ. Wang et al. [27] investigated the effects of nanosecond pulsed laser beam jump directions (outside-in and inside-out) and scanning modes (sequential and cyclical scanning) on the morphology of the hole sidewalls in a spiral scanning mode. The results indicate that using the outside-in laser scan path can result in a flatter hole exit morphology at the bottom. Li et al. [28] reported that the interlaced scanning mode can effectively reduce the heat accumulation effect of adjacent trajectories compared with the default sequential scanning mode. Appropriate scanning spacing can balance the two removal mechanisms of laser ablation and mechanical denudation in laser processing [29], and improve the processing quality and efficiency.

In summary, the pulsed laser can achieve better processing quality. Additionally, the spiral scanning method of hole drilling is beneficial in reducing of thermal defects. It is important to note that the carbon fiber absorbs the laser energy best at a wavelength of 1064 nm, and the processing should not consider the resin matrix to absorb the laser energy at this wavelength. Meanwhile, the fiber laser is advantageous due to its high photoelectric conversion efficiency, low cost, and high stability, etc. It is widely used in industrial fields for cutting, hole drilling and other applications. Currently, it is a hot topic for the development of industrial applications. However, the impact of laser parameters on the quality of hole-making for nanosecond pulsed fiber laser drilling of multi-orientation fibers (MD CFRP) has not been adequately studied, and there is still a lack of analysis of the thermal damage pattern resulting from pulsed laser drilling of CFRP.

Therefore, this work employed a 1064 nm nanosecond pulsed fiber laser to create 400 μm diameter micro-holes in 1 mm thick CFRP to investigate the corresponding hole-drilling phenomena and patterns. The study employed a controlled variable method to study the effect of laser processing parameters, including laser power, scan speed, pulse width and laser frequency on the quality of holes produced during the hole drilling process. The quality of micro-holes was assessed based on the diameter of the hole, the HAZ at the entrance and exit, and the taper. The L16 orthogonal experiments were designed to determine the primary factors influencing micro-hole quality based on calculation

**Fig. 1** The system of laser drilling. **a** Structure of CFRP. **b** Schematic diagram of the experimental setup. **c** The path of the scanning mode. **d** Morphology of the focal spot



results. The study also analyzes thermal defects using the microscopic morphology of the micro-hole. This study contributes to optimizing laser hole drilling parameters and provides a theoretical reference for the application of 1064 nm nanosecond pulse laser processing on CFRP.

## 2 Experimental details

### 2.1 Experimental materials and setup

The CFRP specimen is a laminate composed of carbon fiber and epoxy resin matrix. The laminated structure is a multi-layer 0°/90° braided arrangement. Its dimensions are 30 mm × 30 mm × 1 mm (length × width × thickness), as shown in Fig. 1a.

The experimental platform, shown in Fig. 1b, includes a laser, beam splitter, galvanometer, 3D translation stage (with a movement accuracy of 1 μm), power meter, inspiratory device and computer. The pulse nanosecond laser used in this study has a wavelength of 1064 nm and an average power of over 100 W. The pulse width can be adjusted from 2 ns to 500 ns, and the laser frequency is adjustable from 1 kHz to 4000 kHz. The exit beam diameter is 7 mm. A portion of the laser beam is directed toward the power meter through the beam splitter to monitor the laser power in real-time. The remaining portion of the laser enters the galvanometer and is then directed onto the front surface of the CFRP sample using a focusing field lens with a focal length of 200 mm. The CFRP sample is positioned on the sample holder of the 3D translation stage and clamped vertically to minimize the amount of carbon fiber debris adhering to

**Table 1** Hole-drilling parameters of the fiber laser system in the experiment

Characteristics	Symbols	Values	Units
Wavelength	$\lambda$	1064	nm
Average laser power	$P_{avg}$	> 100	W
Focal length	$f$	200	mm
Focused spot diameter	$d_0$	50	μm
Desired hole diameter	$D$	400	μm
Laser power	$P$	93,96,99,102,105	W
Pulse width	$\tau$	6,9,13,20,30	ns
Pulse frequency	$F$	1000,1250,1500,1750,2000	kHz
Scanning speed	$V$	34,42,50,58,66	mm/s

\* $P_{1-5}$  in the table are 93, 96, 99, 102, 105 W, respectively.  $\tau_{1-5}$  are 6,9,13,20,30 ns, respectively.  $F_{1-5}$  are 1000, 1250, 1500, 1750, 2000 kHz, respectively.  $V_{1-5}$  are 34, 42, 50, 58, 66 mm/s, respectively

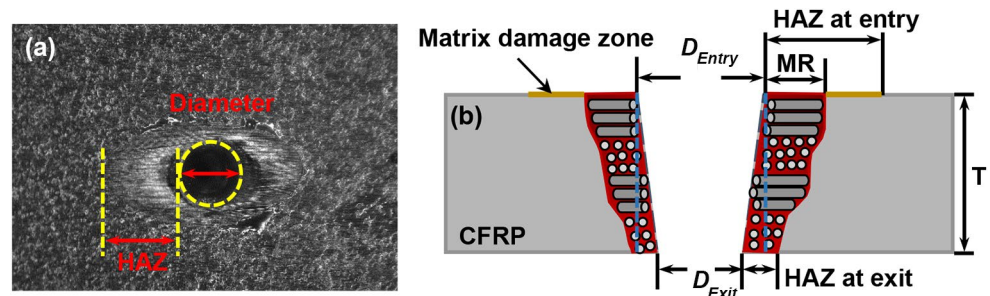
the front surface of the workpiece. To prevent harm to the experimental operators and environmental pollution, an inspiratory device is utilized to pump air onto the front surface of the specimen to filter the smoke and exhaust gases generated during the drilling process. The laser parameters used in the experiments are shown in Table 1.

### 2.2 Experimental strategy

This work focuses on the effects of laser parameters, including power, scanning speed, pulse width, and frequency on the entrance and exit hole diameters, taper, and the HAZ. The experiments utilized a spiral scanning mode and sequence from outside to inside, as illustrated in Fig. 1c. The diameter of the focal spot, measured by the beam quality analyzer, was 50 μm ( $1/e^2$ ), as shown in Fig. 1d. Combined with the

**Table 2** Table of factor levels for orthogonal tests

Level	Factors			
	Laser power P(W)	Scanning speed V(mm/s)	Pulse width $\tau$ (ns)	Laser frequency F(kHz)
1	93	42	6	1250
2	96	50	9	1500
3	99	58	13	1750
4	102	66	20	2000

**Fig. 2** Schematic diagram of micro-hole diameter, HAZ and hole taper. **a** schematic diagram of material surface. **b** schematic diagram of the material cross-section.  $D_{Entry}$  and  $D_{Exit}$  are the entry and exit hole diameters, respectively. MR refers to the matrix recession zone

energy distribution of the beam, the fixed pitch during scanning is  $20\ \mu\text{m}$  ( $d$ ), resulting in a path overlap of 60%.

A single-factor experimental method was used to analyze the influence of the laser parameters on the hole quality. A four-factor, four-level L16 orthogonal design experiment was designed based on the results of the single-factor experiment. It aimed to determine the primary and secondary relationships between power, scanning speed, pulse width, and frequency on hole quality. Table 2 shows the design of the experiment. Each group of parameters was repeated at least three times to avoid contingency in the results.

### 2.3 Measurement/Characterization

The entrance and exit diameters of the micro-holes produce a certain diameter difference, which is expressed as a tapered hole. The diameter difference is influenced by factors such as the distribution of the laser beam and the thickness of the sample, the calculation formula [28, 30] is:

$$t = \frac{D_{Entry} - D_{Exit}}{T} \quad (1)$$

where  $t$  is the hole taper,  $D_{Entry}$  and  $D_{Exit}$  are the entry and exit hole diameters, respectively.  $T$  is the thickness of the CFRP. The experiment defines the magnitude of the variation  $\Delta D$  ( $\Delta D$ ) as the difference in hole diameter of the micro-holes obtained for adjacent laser parameters under the same single factor variation. The calculation equation is as follows:

$$\Delta D_{Entry} = D_{Entry}(X_j) - D_{Entry}(X_i) \quad (2)$$

$$\Delta D_{Exit} = D_{Exit}(X_j) - D_{Exit}(X_i) \quad (3)$$

where  $\Delta D_{Entry}$  and  $\Delta D_{Exit}$ ,  $\Delta D_{Entry}$ ,  $\Delta D_{Exit}$  represent the variation in entry and exit hole diameters, respectively.  $X$  is a single dependent variable parameter, including laser power ( $P$ ), pulse width ( $\tau$ ), frequency ( $F$ ) and scanning speed ( $V$ ). The variables  $i$  ( $i=1,2,3,4,5$ ) and  $j$  ( $j=2,3,4,5$ ) are consecutive numbers of variable parameters. Details are given in the accompanying notes to Table 1.

The thermal conductivity of CFRP is anisotropic. It is higher in the parallel direction,  $50\ \text{W}/(\text{m}\cdot\text{K})$ , compared to  $5\ \text{W}/(\text{m}\cdot\text{K})$  in the vertical direction [19]. Therefore, the inspection focused on the HAZ with the laser scanning direction perpendicular to the carbon fiber, as illustrated in Fig. 2a. Based on this figure, the physical model of the micro-holes cross-section shown in Fig. 2b was defined. The matrix recession (MR) zone is the region where the laser energy is ineffective in removing the carbon fibers at the edge of the hole, but can erode the resin matrix and expose the carbon fibers [32]. The matrix damage zone is the region away from the micro-holes, where the heat conduction effect is ineffective to remove the resin, but may still cause some damage to the resin matrix. This study defines HAZ as the sum of MR and matrix damage zone [26]. Meanwhile, hole diameters at the entrance and exit, as well as the corresponding HAZ width, were observed and measured using a stereomicroscope, as shown in Fig. 2. During the actual measurement of HAZ, the observation of the matrix damage zone was not evident. Multiple measurements were taken for each group of data, and the average value was selected for statistical analysis. The morphology of the micro-holes was measured and the thermal damage defects were analyzed using scanning electron microscopy (SEM).



### 3 Results and discussion

#### 3.1 Laser parameters versus hole diameter

Figures 3 and 4 show the morphologies of the entrance and exit micro-hole obtained for various laser parameters, respectively. It is evident that  $D_{Entry}$  is consistently larger than  $D_{Exit}$  for different laser parameters. This is due to the Gaussian distribution of the laser beam and focal plane being maintained at the front surface during hole drilling, leading to a decrease in laser energy density with increasing depth. Furthermore, the high-energy laser causes both evaporation and burning of the material as it moves along the scan path. The resulting ablative debris carries away some of the heat. Additionally, any ablation material that accumulates around the hole wall and is not removed in time can block some of the laser energy, creating a shielding effect that reduces the energy absorbed by the material along the depth of the hole.

Figure 3 shows the expansion of the fractured fiber ends and the convexity of the carbon fiber layers around the micro-hole, which is directly related to the significant thermal expansion of the carbon fiber and the superposition of thermal deformation of the individual fiber layers. Meanwhile, the HAZ formed during laser irradiation caused the carbon fibers to become loose due to the lack of resin reinforcement, which led to phenomena such as carbon

fiber pull-out and pick-up, as shown in Fig. 3d and h. These effects become more pronounced with increasing laser power, pulse width and frequency, and decreasing scanning speed. Furthermore, during in the experiment, the vaporized material undergoes filtration through pumping. However, it is important to note that the suction of this device may cause the carbon fibers to be picked up and reattached to the surface. On the other hand, as depicted in Fig. 4, only the broken carbon fibers were picked up on the rear surface, as shown in Fig. 4c, and no pulling out of the carbon fiber occurred. This could be attributed to the reduced energy absorbed by the material and the area of influence of the HAZ.

For any combination of laser parameters, all of the micro-holes in Fig. 3 contain the notched profile edges as indicated by the arrows in Fig. 3a. This is due to the spiral scan path starting without overlapping with adjacent spirals, creating a distance gap between the scan spacing as shown in Fig. 1b, which causes a defect in the drilling process. The gap may not be as apparent in some images due to varying amounts of heat accumulation caused by different laser parameters.

The irregular contours and elliptical shapes of the micro-holes on the rear surface, shown in Fig. 4 are due to the reduced energy absorption in the thickness direction of the material, laser dispersion outside the focal plane, changes in thermal conductivity in the fiber direction, and high

**Fig. 3** Micrograph of the holes at the front surface. **a-e**  $V=50$  mm/s,  $\tau=13$  ns,  $F=1500$  kHz,  $P=93-105$  W. **f-j**  $P=99$  W,  $V=50$  mm/s,  $F=1500$  kHz,  $\tau=6-30$  ns. **k-o**  $P=99$  W,  $V=50$  mm/s,  $\tau=13$  ns,  $F=1000-2000$  kHz. **p-t**  $P=99$  W,  $\tau=13$  ns,  $F=1500$  kHz,  $V=34-66$  mm/s. The changed parameters are placed below the corresponding images

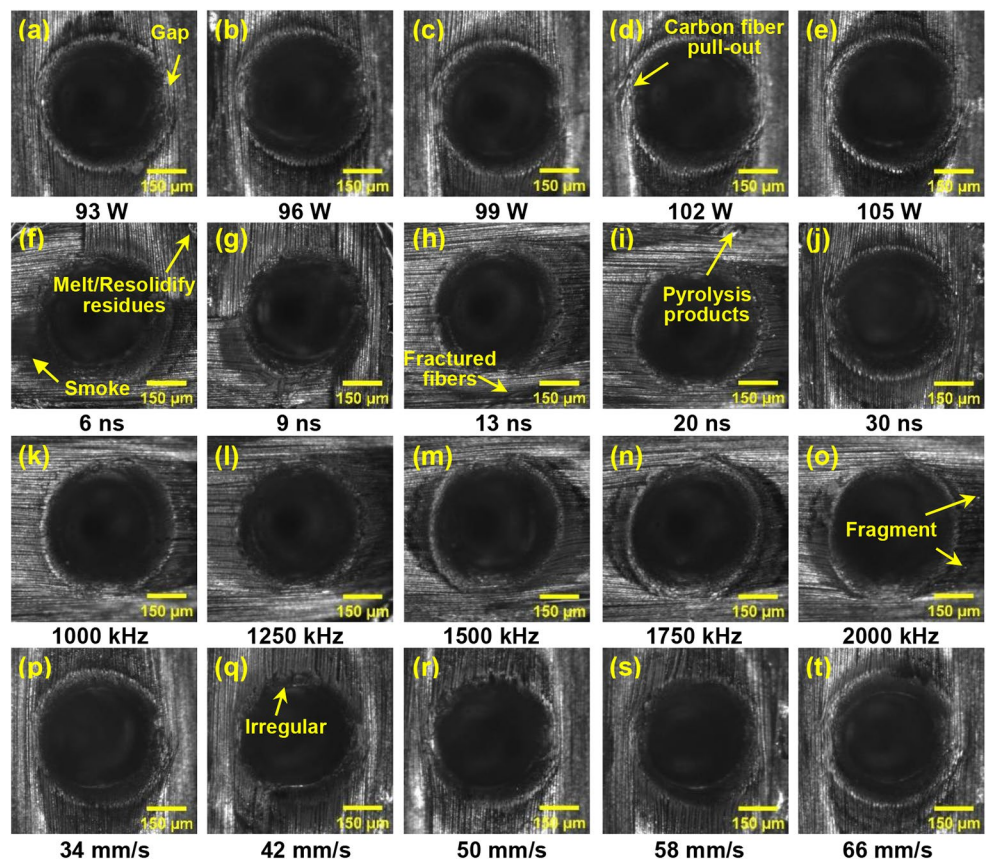
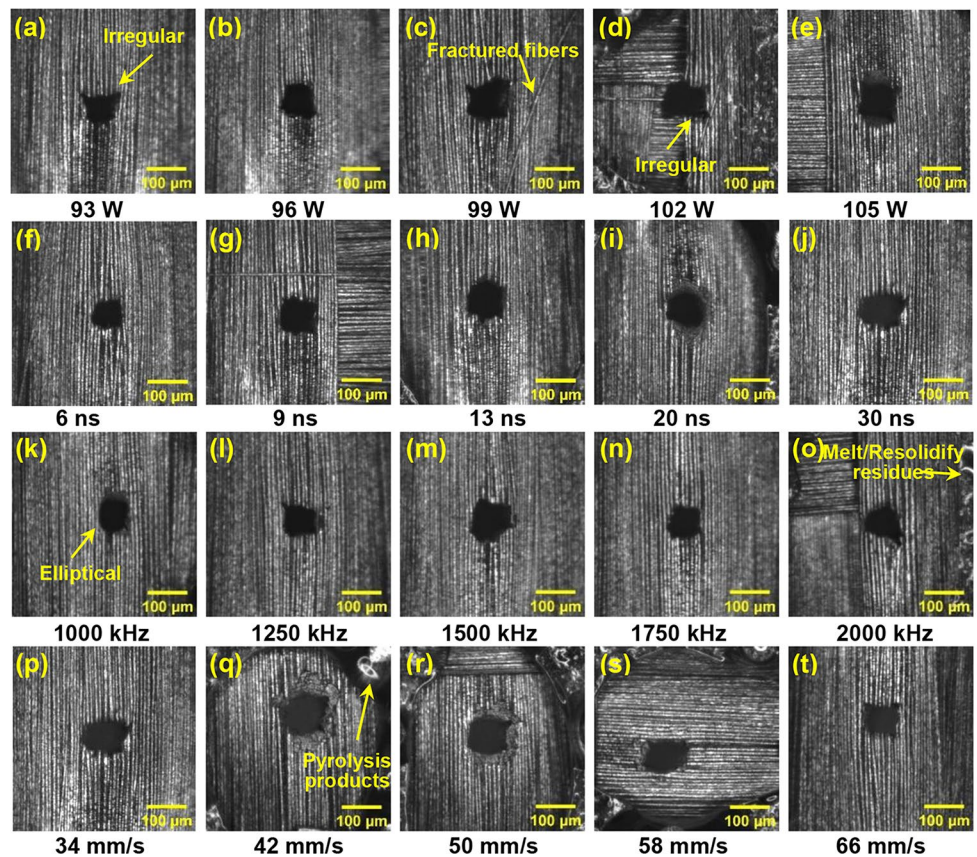


**Fig. 4** Micrograph of the holes at the rear surface. **a–e**  $V=50$  mm/s,  $\tau=13$  ns,  $F=1500$  kHz,  $P=93$ – $105$  W. **f–j**  $P=99$  W,  $V=50$  mm/s,  $F=1500$  kHz,  $\tau=6$ – $30$  ns. **k–o**  $P=99$  W,  $V=50$  mm/s,  $\tau=13$  ns,  $F=1000$ – $2000$  kHz. **p–t**  $P=99$  W,  $\tau=13$  ns,  $F=1500$  kHz,  $V=34$ – $66$  mm/s. The changed parameters are placed below the corresponding images



processing temperatures [18]. The circularity of the micro-holes on the rear surface is much smaller than that of the front surface. Meanwhile, the energy absorbed at the rear surface of the material is insufficient to directly vaporize the resin matrix. Additionally, the temperature of heat transfer through carbon fibers is also lower than the vaporization temperature of the resin. However, it has reached its liquefaction phase transition temperature, resulting in a residue of pyrolysis and melting, followed by re-curing in the area near the micro-holes on the rear surface, as shown in Fig. 4o and q.

Figure 5 shows the quantitative relationship between the hole diameter at the entrance and exit of the micro-hole and the laser parameters shown in Figs. 3 and 4. The hole diameter at both  $D_{Entry}$  and  $D_{Exit}$  increase with increasing laser power, pulse width and frequency increase, and decreasing scanning speed. This relationship is directly linked to the material removal rate. As the laser power and pulse width increase, the material is melted and vaporized, enhancing material removal capability. It results in larger hole diameters for  $D_{Entry}$  and  $D_{Exit}$ . Laser frequency and scanning speed also affect the interaction time between the laser and the CFRP material. The time taken to heat the material increases as the laser frequency increases and the scanning

speed decreases, resulting in more material being removed and an increase in the diameter of the entry and exit holes.

The objective of the study is to achieve a micro-hole diameter of  $400 \mu\text{m}$ . The impact of the parameter on hole quality is quantified using the quality factor ‘ $Q$ ’. The  $Q$  at the entrance ( $Q_{Entry}$ ) is defined as the ratio of the actual entrance hole diameter ( $D_{Entry}$ ) to the desired diameter ( $D_{Entry}/D$ ). Figure 5 shows the relationship between laser power, pulse width, laser frequency, scanning speed and  $Q_{Entry}$ . It is shown that the variation range of  $Q_{Entry}$  ranges from 0.981 to 1.157 when altering the laser power, from 0.970 to 1.121 when adjusting the pulse width, from 0.972 to 1.090 when modifying the laser frequency, and from 0.959 to 1.125 when varying the scanning speed. Overall,  $Q_{Entry}$  increases as laser power, pulse width and laser frequency increase, and as scanning speed decreases. This is consistent with the variation of  $D_{Entry}$ .

$Q_{Entry}$  values of 1.003, 0.996, 0.989 and 1.010 were obtained when the laser power was 96 W, the pulse width was 9 ns, the laser frequency was 1250 kHz and the scanning speed was 50 mm/s, respectively. The  $Q_{Entry}$  of all sites approaches 1, indicating that the  $D_{Entry}$  of the micro-hole obtained under this parameter is closest to  $D$ . The quality factor at the exit is not discussed in these experimental results because the  $D_{Exit}$  at either laser variable parameter



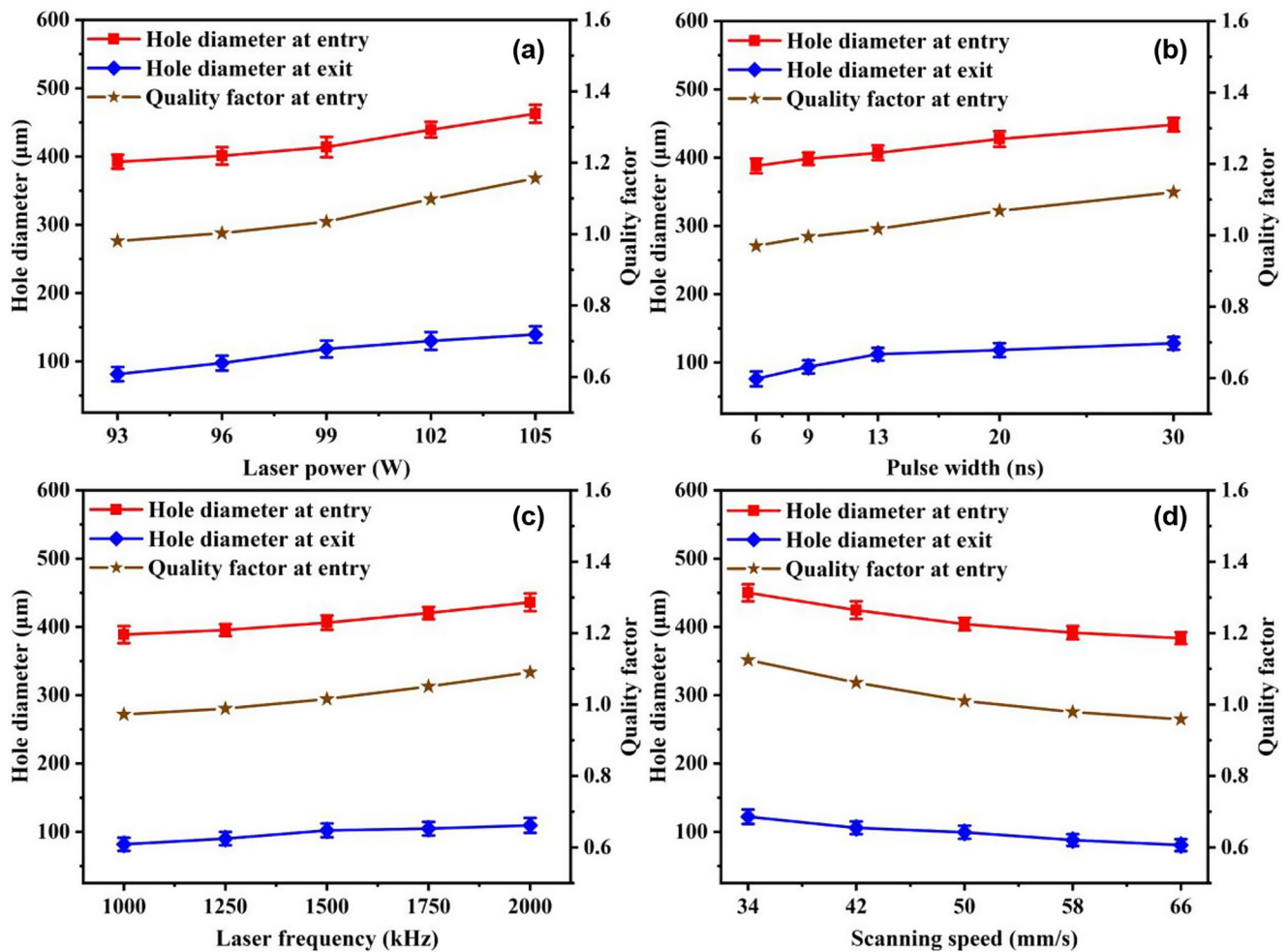


Fig. 5 Hole diameter at the entry ( $D_{Entry}$ ) and exit ( $D_{Exit}$ ) and quality factor at entry ( $Q_{Entry}$ ) versus laser parameters

is significantly smaller than  $D$ . The study used a forward pumping process that weakened the ability of the laser energy to interact with the thickness of the CFRP in the direction of the thickness. Additionally, the shielding effect of laser energy blocks and scatters the laser beam, reducing the amount of material removal at the exit of the micro-hole, which leads to the reduction in laser processing accuracy at the exit of the micro-hole.

### 3.2 Laser parameters versus taper

Figure 6a-f show the relationship between the taper and the laser parameters in Figs. 3 and 4, along with the corresponding variation curves of  $D_{Entry}$  and  $D_{Exit}$ . The exit diameter ( $\Delta D_{Exit}$ ) shows a larger variation range than the entry diameter ( $\Delta D_{Entry}$ ) when the laser power, pulse width and laser frequency are changed. However, the opposite pattern is observed when the scanning speed is changed.

Based on Eq. (1), the magnitude of the taper is primarily determined by the difference in diameter at the entry and

exit when the material thickness  $T$  is constant. Figure 6a-f demonstrate that the smallest taper is achieved at 99 W power, 13 ns pulse width and 1500 kHz frequency, resulting in values of 0.296, 0.295 and 0.304, respectively. Increasing the power, frequency and pulse width leads to a larger taper. Figure 6g and h demonstrate that the taper gradually decreases as the scanning speed increases, leveling off at 50 mm/s. This is because  $\Delta D_{Exit}$  is always greater than  $\Delta D_{Entry}$ . Once the speed is increased to 50 mm/s, the variation of the  $D_{Entry}$  and  $D_{Exit}$  becomes similar, resulting in a micro-hole with a taper of 0.295. In summary, changing the laser power, pulse width and laser frequency results in the same variation trend for the taper. By altering the scanning speed, the opposite trend can be achieved.

It is evident that when the laser power, pulse width and frequency are increased to a certain threshold, the energy absorbed by the material on the rear surface fluctuates significantly. This results in an increase in the energy utilization of the material removed from the rear surface, and  $\Delta D_{Entry}$  is smaller than  $\Delta D_{Exit}$ . However, as the value of the

**Fig. 6** Relationship between taper and laser parameters. **a, c, e** and **g** indicate the relationship between taper and laser parameters, respectively. **b, d, f** and **h** indicate the relationship between  $\Delta D$  and laser parameters respectively.  $X_{ji}$  in the figure is indicated as the difference between adjacent values of single dependent variable parameter

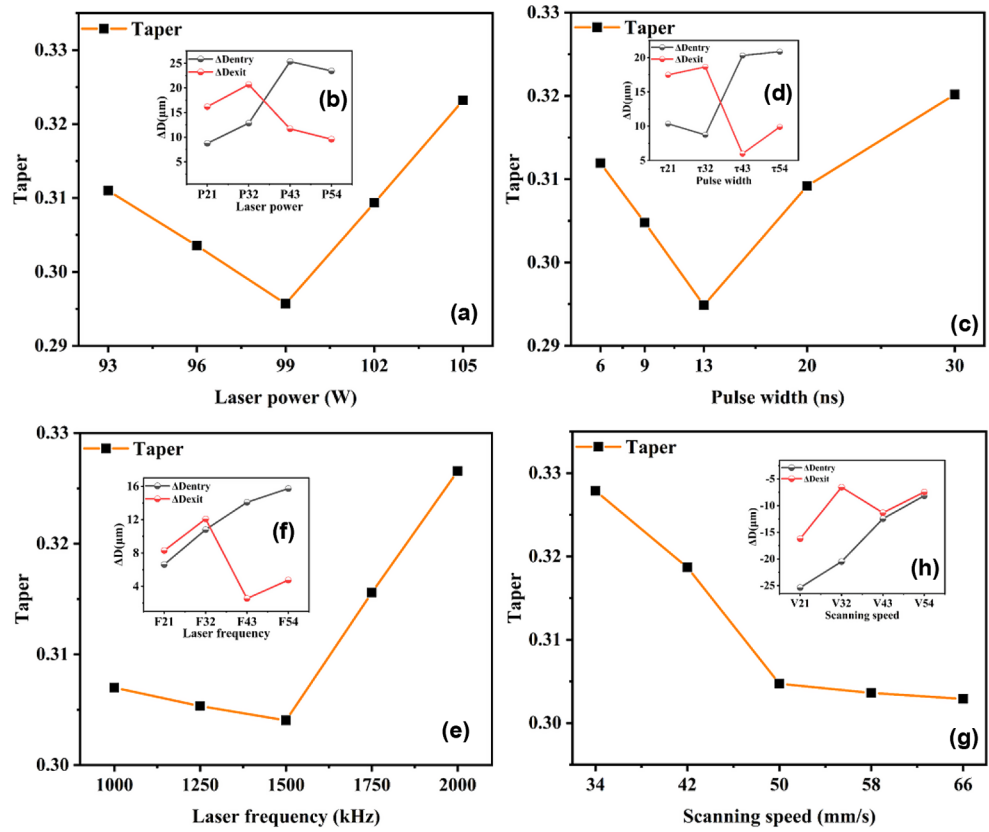
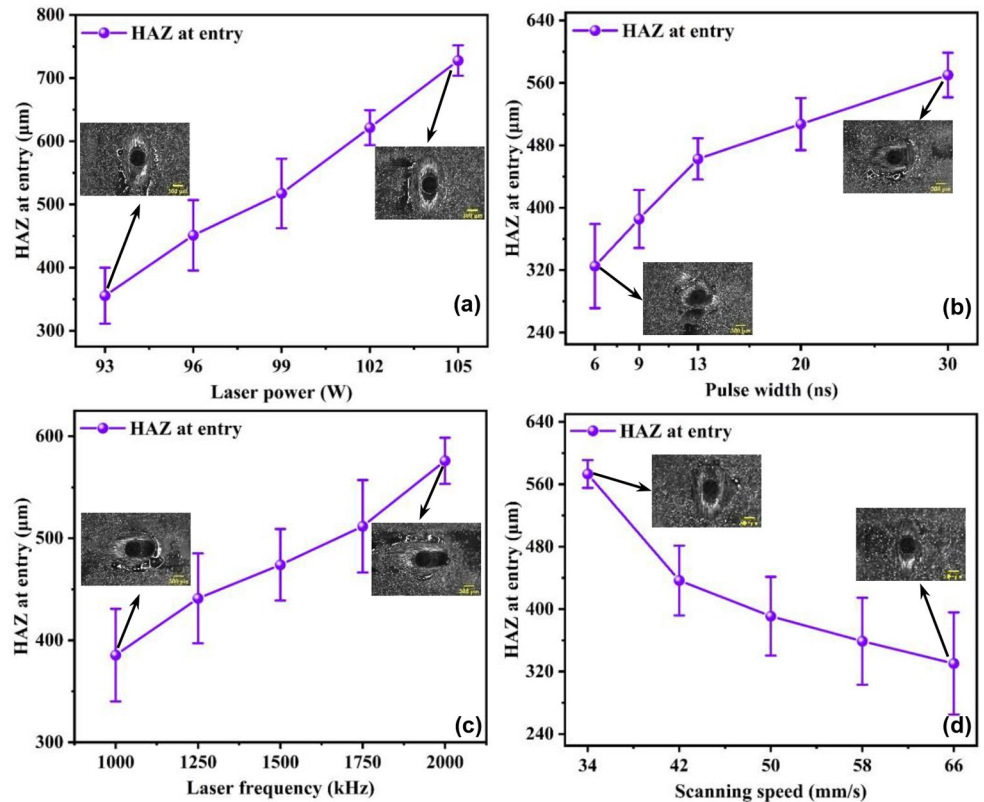


**Fig. 7** HAZ at the entry in relation to laser parameters





laser variable parameter continues to increase, the plasma shielding effect of the front surface increases. This results in more intense ablation, increased material removal, and a significant increase in  $D_{Entry}$ . In contrast, the rear surface absorbs relatively little energy, limiting material removal, and resulting in a relatively stable trend of increasing  $D_{Exit}$ . This indicates that the hole taper can be increased by using too much or too little laser power, pulse width and frequency. The micro-hole obtained in this experiment had a taper of approximately 0.3 when the laser parameters were set to 99 W, 50 mm/s, 13 ns, and 1500 kHz.

### 3.3 Laser parameters versus HAZ

CFRP is an anisotropic material composed of carbon fiber and epoxy resin, which have significantly different thermal properties. Carbon fibers have a much higher vaporization temperature (3900 K) and better thermal conductivity than epoxy resin (698 K) [19]. When laser irradiates CFRP, the material absorbs heat, causing the epoxy resin to reach the vaporization temperature earlier. As a result, the resin matrix is removed first, exposing the unremoved carbon fibers and forming a HAZ.

Figure 7a shows that an increase in laser power results in an increase in the heat absorbed per unit of time on the surface material. However, the carbon fiber material in the center of the micro-hole is removed, and the heat accumulation around the micro-hole also increases. Although it does not reach the vaporization temperature, it already far exceeds the vaporization temperature of the resin matrix, causing the heated vaporization area to expand further, which in turn leads to a gradual expansion of the width of the HAZ at the entrance ( $HAZ_{Entry}$ ). Increasing pulse width resulting in

longer heating time for the carbon fiber material and shorter cooling time, which can lead to heat accumulation in the irradiated area, resulting in the HAZ variation shown in Fig. 7b.

The effects of laser frequency and scanning speed on the HAZ are shown in Fig. 7c and d, respectively. These effects are due to the two parameters affecting the laser spot overlap rate. According to the formula:

$$\varphi = \left(1 - \frac{V}{d \times F}\right) \times 100\% \quad (4)$$

The variables used in Eq. (4) are beam overlap rate ( $\varphi$ ), the scanning speed ( $V$ ), the spot diameter ( $d$ ) and the laser frequency ( $F$ ), respectively. The  $\varphi$  is directly proportional to the  $F$  and inversely proportional to the  $V$  when the  $d$  remains constant. To effectively reduce heat accumulation in the processed material, and minimize the size of the HAZ, it is recommended to decrease the frequency or increase the scanning speed. This will help to minimize the HAZ. Additionally, decreasing the time between adjacent pulses by increasing the laser frequency, while keeping the pulse width constant, can further reduce cooling time in the processed area.

Figure 7 illustrates the relationship between  $HAZ_{Entry}$  and laser parameters. It shows that the  $HAZ_{Entry}$  increases with laser power, pulse width and frequency, and decreases with scanning speed. The SEM image given in Fig. 8 demonstrates that these parameter changes result in more carbon fiber fracture around the micro-holes, increased fiber tip swelling, significant carbon fiber pull-out, and the formation of obvious cracks and striations. Meanwhile, ablation debris and matrix degradation residues adhere to the raised

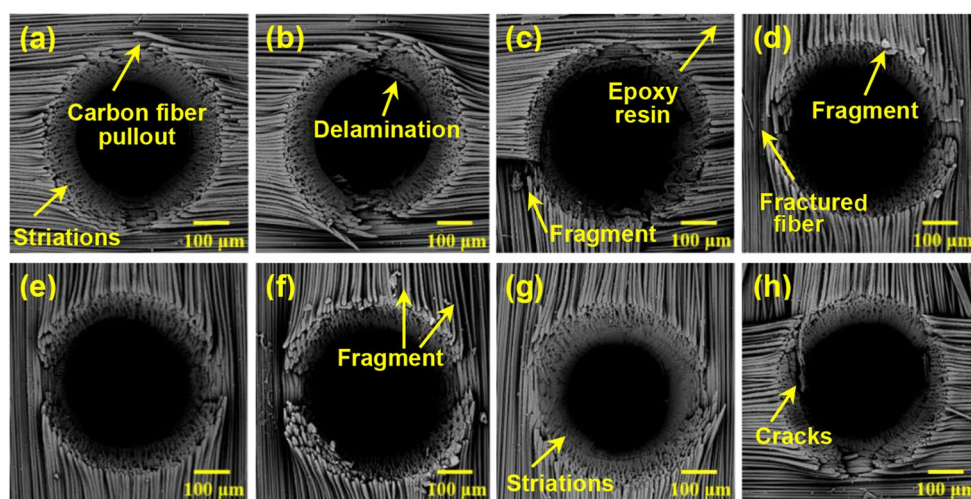


**Fig. 8** SEM micrographs at the entry of the micro-hole with different laser parameters. **a**  $P=93$  W,  $V=50$  mm/s,  $\tau=13$  ns,  $F=1500$  kHz. **b**  $P=105$  W,  $V=50$  mm/s,  $\tau=13$  ns,  $F=1500$  kHz. **c**  $P=99$  W,  $V=50$  mm/s,  $\tau=6$  ns,  $F=1500$  kHz. **d**  $P=99$  W,  $V=50$  mm/s,  $\tau=30$

ns,  $F=1500$  kHz. **e**  $P=99$  W,  $V=50$  mm/s,  $\tau=13$  ns,  $F=1000$  kHz. **f**  $P=99$  W,  $V=50$  mm/s,  $\tau=13$  ns,  $F=2000$  kHz. **g**  $P=99$  W,  $V=34$  mm/s,  $\tau=13$  ns,  $F=1500$  kHz. **h**  $P=99$  W,  $V=66$  mm/s,  $\tau=13$  ns,  $F=1500$  kHz

carbon fibers, affecting the mechanical strength and properties of the CFRP.

Figure 9 shows the relationship between the width of the HAZ at the exit ( $HAZ_{Exit}$ ) and the laser parameters. The  $HAZ_{Exit}$  is larger than the  $HAZ_{Entry}$  when the power is 93 W power, the pulse width is  $\leq 9$  ns and the scan speed is  $\geq 58$  mm/s. Otherwise, the  $HAZ_{Exit}$  is smaller than the  $HAZ_{Entry}$ . Figure 9a shows that the  $HAZ_{Exit}$  first increases and then decreases with increasing laser power, with the maximum  $HAZ_{Exit}$  (441.163  $\mu\text{m}$ ) obtained at 96 W laser power. The  $HAZ_{Exit}$  reaches its minimum value (377.022  $\mu\text{m}$ ) for laser power of 102 W. Figure 9b shows that the  $HAZ_{Exit}$  decreases and then increases with increasing pulse width, with a minimum value  $HAZ_{Exit}$  (325.942  $\mu\text{m}$ ) obtained at a pulse width of 13 ns. The rate of increase slows down for the pulse width greater than 20 ns.

Figure 9c shows that the maximum  $HAZ_{Exit}$  is achieved at a laser frequency of 1500 kHz. As the frequency increases,  $HAZ_{Exit}$  decreases significantly. At a frequency of 2000 kHz, the  $HAZ_{Exit}$  is 312.765  $\mu\text{m}$ . Similarly, the effect of the scanning speed is comparable to that of the pulse width, and Fig. 9d shows that the smallest HAZ (268.366  $\mu\text{m}$ ) is achieved at a scanning speed of 50 mm/s.

The variation of  $HAZ_{Exit}$  is primarily determined by whether the material absorbs enough energy to reach the carbon fiber ablation condition when the laser parameters are changed. The relationship between each parameter and the energy remains consistent, as described in Sect. 3.1.

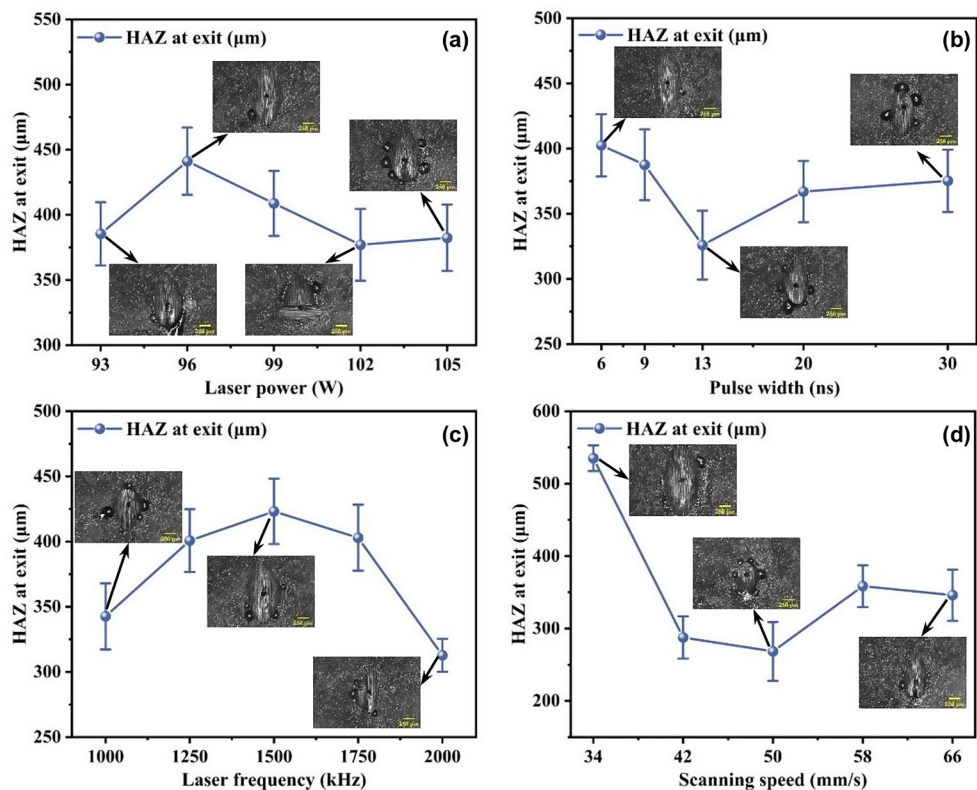
When the energy reaches the carbon fiber ablation condition, the energy utilization increases and the energy used for heat transfer dissipation decreases, resulting in a decrease in  $HAZ_{Exit}$ . However, if the absorbed energy is insufficient to remove the carbon fibers, the heat will evaporate the resin through the carbon fiber heat transfer, which will increase the  $HAZ_{Exit}$ . In addition, if the energy density is too high, the epoxy resin matrix will be removed by both direct vaporization and indirect ablation by heat conduction, resulting in an even greater  $HAZ_{Exit}$ .

The range of the HAZ shown in Figs. 7 and 9 fluctuates considerably. It is because the thermal conductivity of carbon fibers is 10 times higher along the radial direction than in the axial direction [19]. As a result, heat is primarily transmitted along the radial direction and diffuses into the interior of the material. Despite this, the total energy input remains constant, resulting in an elliptical heat-affected zone. The extent of the HAZ varies greatly for micro-holes obtained with the same parameters due to the different contact locations of the laser beam on the material and the anisotropy of the carbon fibers. This variation is caused by the laser irradiating carbon fibers with different weave orientations.

### 3.4 Micro-hole sidewall morphology and defects

Figure 10 shows the morphology of the micro-hole sidewall under different laser parameters. The micro-holes exhibit

**Fig. 9** HAZ at the exit in relation to laser parameters



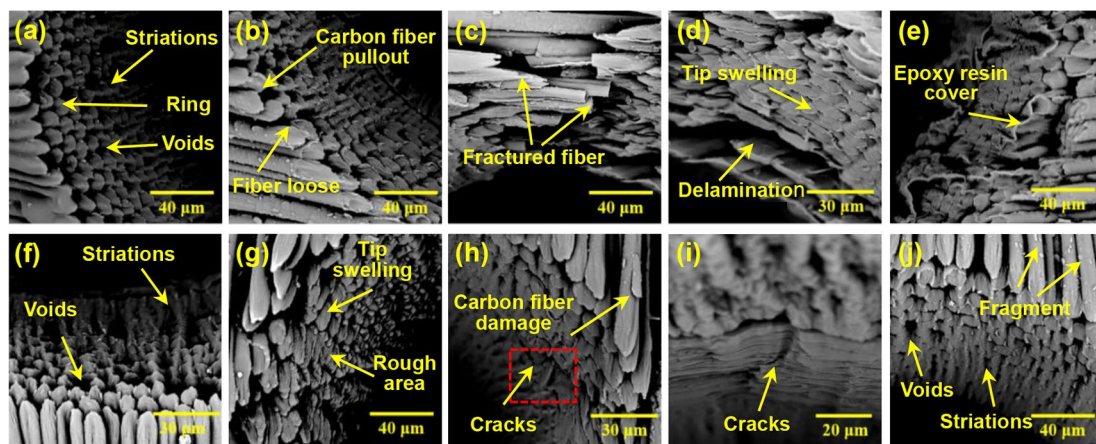
striations, voids, fiber pull-out, rings, fiber fractures, tip swelling, fiber delamination, epoxy resin coverage, and fragments. These features result in multi-physical complexities, including rough surface formation, fiber damage, and interlayer cracks on the sidewall surface.

Figure 10a shows striations and voids on the sidewall of the micro-holes for each combination of laser parameters. Negarestani et al. [31] attributed the striations to the unsteady motion of pyrolysis products of the epoxy, such as light gases, various hydrocarbons, and carbon. It was found that the number of striations and voids in Fig. 10f and j increased significantly when the laser frequency was less than 1000 kHz and the scanning speed was greater than 66 mm/s. This is attributed to the low overlap rate between adjacent pulse spots at these laser parameters, which results in the presence of an incomplete removal area between the materials such that striations are visible. Voids are the thermal defects that occur during the ablation of the resin matrix, resulting in matrix loss [26]. During laser irradiation, the energy used to reach the carbon fiber ablation threshold is reduced, resulting in more energy being dissipated by heat conduction rather than material removal. This leads to the resin matrix being ablated over a wider temperature range, resulting in an increased number of surface voids. It has been found that the number of voids decreases as the hole depth increases. This phenomenon can be attributed to two main reasons. Two main factors contribute to the increased ablation of the epoxy resin matrix in the micro-hole. Firstly, the absorption of laser energy is greater near the entrance of the hole, causing inconsistent vaporization temperatures of the carbon fiber and resin, and significant heat accumulation between unremoved carbon fibers. Secondly, the shrinkage of the surface fiber ends leads to the increased formation of voids. Meanwhile, Fig. 10a and other figures show

varying degrees of rings in the center of the fiber end. This is related to the radial thermal melting of the carbon fiber [32]. The degree of thermal melting varies with different energy parameters and the formation of rings varies.

In addition, loosening occurs in the area near the surface of the micro-hole shown in Fig. 10b, and the outer carbon fibers are easily pulled out. This phenomenon becomes more pronounced as the laser power, pulse width, and frequency increase and the scanning speed decreases. This is related to the thermal deformation of the carbon fiber between the layers and the use of suction at the entrance. The suction remove heat from the hole and carries it away to the entrance surface, which exacerbates the heat accumulation effect within the entrance region. In addition, Fig. 10c shows that the laser scanning direction removes a greater amount of material parallel to the carbon fiber direction compared to the perpendicular direction. This results in more fractured and damaged carbon fibers. This is due to the higher heat conductivity along the carbon fiber direction than in the vertical direction.

As the power, pulse width and frequency increase and the scanning speed decreases, the number of delamination and cracks in Fig. 10d-h increases, and the epoxy resin covering the processing section and wrapping the carbon fiber gradually disappears. This is related to the increase of laser energy and heat accumulation. When the laser frequency reaches 2000 kHz, the processed cross-section shows a rough and uneven area shown in Fig. 10g, and the fiber ends are already slightly swollen. This may be related to thermal damage caused by shortened cooling time or may be caused by incomplete thermal fusion occurring between carbon fibers [32]. At scanning speed below 34 mm/s, significant ‘fish scale’ peel damage and micro-cracks appear on the surface of the carbon fiber as shown in Fig. 10h.



**Fig. 10** SEM morphology of the sidewall of the micro-hole obtained with different laser parameters. **a** $P=93$  W,  $V=50$  mm/s,  $\tau=13$  ns,  $F=1500$  kHz. **b** $P=99$  W,  $V=50$  mm/s,  $\tau=13$  ns,  $F=1500$  kHz. **c**, **d** $P=105$  W,  $V=50$  mm/s,  $\tau=13$  ns,  $F=1500$  kHz. **e** $P=99$  W,  $V=50$  mm/s,  $\tau=6$  ns,  $F=1500$  kHz. **f** $P=99$  W,  $V=50$  mm/s,  $\tau=13$

ns,  $F=1000$  kHz. **g** $P=99$  W,  $V=50$  mm/s,  $\tau=13$  ns,  $F=2000$  kHz. **h** $P=99$  W,  $V=34$  mm/s,  $\tau=13$  ns,  $F=1500$  kHz. **i** is an enlarged image of the boxed area in **h**. **j** $P=99$  W,  $V=66$  mm/s,  $\tau=13$  ns,  $F=1500$  kHz



A magnified image of the box in Fig. 10h is presented in Fig. 10i. These phenomena are mainly caused by thermal damage defects resulting from prolonged laser scanning of the CFRP surface.

The results of morphological analysis indicate that the use of 99 W, 50 mm/s, 13 ns, and 1500 kHz to drill the holes does not alter the carbon fiber arrangement, resulting in reduced thermal damage and machining defects. In addition, this combination of parameters leads to smaller  $t$  and HAZ.

### 3.5 Orthogonal test results and analysis

Table 3 shows the experimental results obtained from the four-factor, four-level L16 orthogonal design. The statistical results shown in Table 4 are obtained based on the experimental data in this table. When evaluating the hole quality using  $D_{Entry}$ ,  $D_{Exit}$ ,  $HAZ_{Entry}$ ,  $HAZ_{Exit}$  and  $t$  as indicators, the laser power has the greatest effect on  $D_{Entry}$ , followed by scanning speed, pulse width, and laser frequency. The impact of laser parameters on  $HAZ_{Entry}$  is as follows: laser power has the greatest effect, followed by pulse width, laser frequency, and scanning speed. Laser power is the primary factor influencing  $D_{Entry}$  and  $HAZ_{Entry}$ . This is because power directly affects the energy density of the beam. The higher the energy density, the more energy is absorbed by the CFRP material, making it easier to remove and directly affecting the hole diameter and HAZ at the entrance. Laser frequency has no significant effect on  $D_{Entry}$ . It can be adjusted to obtain the minimum  $Q_{Entry}$  variation range.

The effect of laser parameters on  $D_{Exit}$  is in the following order: pulse width, scanning speed, laser power, and laser frequency. The impact of laser parameters on  $HAZ_{Exit}$  and  $t$  is in the following order: pulse width, laser power, scanning

speed, and laser frequency. It is evident that the pulse width has a significant effect on  $D_{Exit}$ ,  $HAZ_{Exit}$  and  $t$ . Additionally, the pulse width affects the energy density. Furthermore, the pulse width is linked to the duration of interaction between the laser and the CFRP material. A larger pulse width leads to a longer interaction time in the thickness direction, resulting in reduced cooling time, and increased heat accumulation. This, in turn, causes notable variations in the hole diameter and HAZ, as well as in the taper at the exit. It is inconsistent with the conclusion of reference [19] that pulse width has the most significant effect on each quality factor. It may be related to the small range of pulse width in this orthogonal experiment. Meanwhile, Zhou et al. [19] used a pulse width of 0.1–0.25 ms, which is much larger than the pulse width used in this work. A larger pulse width of the laser inevitably leads to a larger thermal effect. In addition, the outward pumping method used for laser drilling of CFRP in this work interferes with the direction of heat conduction at the entrance of the sample, which negatively impacts the quality of holes.

## 4 Conclusions

A drilling study was conducted on the surface of CFRP using a 1064 nm nanosecond pulsed fiber laser, based on the univariate variables and orthogonal design experiments. The effects of laser parameters, including laser power, pulse width, laser frequency and scanning speed, on the processing quality were analyzed. The conclusions are as follows:

(1) The diameter of micro-holes and the width of the HAZ vary positively with laser power, pulse width and frequency, and inversely with scanning speed. To obtain a hole surface without smoke accumulation at the entrance,

**Table 3** Orthogonal test results of laser drilling CFRP

No	$P$ (W)	$V$ (mm/s)	$\tau$ (ns)	$F$ (kHz)	$D_{Entry}$ ( $\mu\text{m}$ )	$D_{Exit}$ ( $\mu\text{m}$ )	$HAZ_{Entry}$ ( $\mu\text{m}$ )	$HAZ_{Exit}$ ( $\mu\text{m}$ )	$t$
1	1	1	1	1	399.089	23.844	397.089	109.352	0.375
2	1	2	2	2	395.471	70.334	339.693	317.749	0.325
3	1	3	3	3	394.648	74.990	431.025	271.183	0.320
4	1	4	4	4	393.053	45.882	340.207	222.372	0.347
5	2	1	2	3	401.835	77.305	413.099	318.725	0.325
6	2	2	1	4	392.151	51.852	494.451	156.090	0.340
7	2	3	4	1	374.380	52.343	468.126	346.405	0.322
8	2	4	3	2	383.515	43.447	470.184	144.943	0.340
9	3	1	3	4	378.629	84.316	456.716	429.188	0.294
10	3	2	4	3	385.920	64.818	426.567	341.924	0.321
11	3	3	1	2	390.027	31.793	487.492	140.121	0.358
12	3	4	2	1	381.477	39.931	474.553	222.294	0.342
13	4	1	4	2	388.161	113.963	445.590	520.284	0.274
14	4	2	3	1	383.648	92.678	450.315	507.638	0.291
15	4	3	2	4	383.997	76.126	400.401	368.608	0.308
16	4	4	1	3	374.394	35.314	380.850	237.687	0.339



**Table 4** Average response calculated based on orthogonal experimental level design

Levels	<i>P</i>	<i>V</i>	$\tau$	<i>F</i>	Levels	<i>P</i>	<i>V</i>	$\tau$	<i>F</i>
<i>D<sub>Entry</sub></i>					<i>D<sub>Exit</sub></i>				
1	395.565	391.928	388.915	384.648	1	53.762	74.857	35.701	52.199
2	387.97	389.297	390.695	389.293	2	56.237	69.92	65.924	64.884
3	384.013	385.763	385.11	389.199	3	55.215	58.813	73.858	63.107
4	382.55	383.11	385.378	386.957	4	79.52	41.144	69.251	64.544
Delta	13.015	8.819	5.585	4.645	Delta	25.758	33.713	38.157	12.685
Rank	1	2	3	4	Rank	3	2	1	4
<i>HAZ<sub>Entry</sub></i>					<i>HAZ<sub>Exit</sub></i>				
1	377.003	428.124	439.97	447.521	1	230.164	344.388	160.813	296.422
2	461.465	427.756	406.936	435.74	2	241.541	330.85	306.844	280.774
3	461.332	446.761	452.06	412.885	3	283.382	281.579	338.238	292.38
4	419.289	416.448	420.122	422.944	4	408.554	206.824	357.746	294.065
Delta	84.462	30.313	45.124	34.635	Delta	178.39	137.564	196.934	15.648
Rank	1	4	2	3	Rank	2	3	1	4
<i>t</i>									
1	0.342	0.317	0.353	0.332					
2	0.332	0.319	0.327	0.324					
3	0.329	0.327	0.311	0.326					
4	0.303	0.342	0.316	0.322					
Delta	0.039	0.025	0.042	0.01					
Rank	2	3	1	4					

the front inspiratory method can be used, although the taper may be larger. The magnitude of the change in the diameter of the entrance and exit holes is closely related to the variation of the taper. When the laser parameters are set to 99 W, 13 ns, 1500 kHz and 50 mm/s, a hole taper of at least 0.3 can be achieved.

(2) Using laser drilling with the front inspiratory process, a laser power is 96 W, pulse width of 9 ns, frequency of 1250 kHz and scanning speed of 50 mm/s results in an entrance diameter closest to the desired diameter, while the exit diameter is significantly smaller than desired.

(3) The heat conduction variability in different directions of the carbon fiber leads to the formation of an elliptical HAZ profile on the micro-hole surface. The width of the *HAZ<sub>Entry</sub>* is significantly increased by the front inspiratory direction. The variation of the *HAZ<sub>Exit</sub>* is related to the use of pulse energy for material removal under different laser parameters.

(4) The drilling process can result in various micro-defects, such as striations, voids, delamination, micro-cracks, carbon fiber ‘fish scale’ peeling damage, fiber pull-out, fiber tip swelling, rings, rough surfaces. The formation of thermal damage defects is closely related to the choice of laser parameters. The use of front pumping at the entrance can exacerbate the micro-hole surface, leading to a protruding layer and fiber pull-out.

(5) The evaluation of drilling quality can be based on indicators such as the *D<sub>Entry</sub>* and *D<sub>Exit</sub>*, the width of the *HAZ<sub>Entry</sub>* and *HAZ<sub>Exit</sub>*, and the taper. Among the various parameters, the laser power is the main factor affecting the *D<sub>Entry</sub>*, and the

*HAZ<sub>Entry</sub>*. On the other hand, the pulse width has a significant effect on the *D<sub>Exit</sub>*, the *HAZ<sub>Exit</sub>* and the taper. It is worth noting that smaller pulse widths have less effect on the quality of the entrance hole. The diameter of the hole is affected by the scanning speed, while the laser frequency does not significantly affect any of the indicators used to evaluate the quality of the hole.

**Author contributions** Xinyi Liu: Writing-original draft, Methodology, Writing-review & editing, Data curation, Formal Analysis, Conceptualization. Sen Yang: Conceptualization, Methodology, Supervision, Formal Analysis. Youdong Gao: Validation, Methodology, Data curation, Visualization, Software. Man Xu: Validation, Conceptualization, Supervision. Yu Wan: Investigation, Validation, Data curation. Meng Wu: Resources, Investigation, Supervision. Lin Li: Investigation, Validation, Data curation. Chenzhuo Wang: Data curation, Conceptualization, Validation. Mian Zhong: Writing-review & editing, Validation, Methodology, Resources. Biyi Wang: Conceptualization, Resources, Validation. Yong Jiang: Writing-review & editing, Project administration, Funding acquisition, Methodology, Supervision.

**Funding** This work was supported by National Natural Science Foundation of China (11972313), Fund Project of Key Laboratory of Electro-Optical Information Control and Security Technology, China (2022JCJQLB055007).

**Declarations**

**Ethical approval** Not applicable.

**Consent to participate** Not applicable.

**Conflict of interest** The authors declare no competing interests.

## References

- Altin Karataş M, Gökçaya H (2018) A review on machinability of carbon fiber reinforced polymer (CFRP) and glass fiber reinforced polymer (GFRP) composite materials. *Def Technol* 14(4):318–326. <https://doi.org/10.1016/j.dt.2018.02.001>
- Alam P, Mamalis D, Robert C, Floreani C, Ó Brádaigh CM (2019) The fatigue of carbon fibre reinforced plastics - a review. *Compos Part B Eng* 166:555–579. <https://doi.org/10.1016/j.compositesb.2019.02.016>
- Dandekar CR, Shin YC (2012) Modeling of machining of composite materials: a review. *Int J Mach Tool Manu* 57:102–121. <https://doi.org/10.1016/j.ijmactools.2012.01.006>
- Scholz MS, Blanchfield JP, Bloom LD, Coburn BH, Elkington M, Fuller JD, Gilbert ME, Muflahi SA, Pernice MF, Rae SI, Trevarthen JA, White SC, Weaver PM, Bond IP (2011) The use of composite materials in modern orthopaedic medicine and prosthetic devices: a review. *Compos Sci Technol* 71(16):1791–1803. <https://doi.org/10.1016/j.compscitech.2011.08.017>
- Poór DI, Geier N, Pereszlai C, Xu J (2021) A critical review of the drilling of CFRP composites: Burr formation, characterisation and challenges. *Compos Part B Eng* 223:109155. <https://doi.org/10.1016/j.compositesb.2021.109155>
- Wang F, Bi G, Ning F (2020) Modeling of dynamic milling forces considering the interlaminar effect during milling multidirectional CFRP laminate. *J Reinf Plast Comp* 40(11–12):437–449. <https://doi.org/10.1177/0731684420971760>
- El-Hofy MH, El-Hofy H (2018) Laser beam machining of carbon fiber reinforced composites: a review. *Int J Adv Manuf Technol* 101(9–12):2965–2975. <https://doi.org/10.1007/s00170-018-2978-6>
- Habib S, Okada A (2016) Influence of electrical discharge machining parameters on cutting parameters of carbon fiber-reinforced plastic. *Mach Sci Technol* 20(1):99–114. <https://doi.org/10.1080/10910344.2015.1133914>
- Yue X, Yang X, Tian J, He Z, Fan Y (2018) Thermal, mechanical and chemical material removal mechanism of carbon fiber reinforced polymers in electrical discharge machining. *Int J Mach Tool Manu* 133:4–17. <https://doi.org/10.1016/j.ijmactools.2018.05.004>
- Shanmugam DK, Nguyen T, Wang J (2008) A study of delamination on graphite/epoxy composites in abrasive waterjet machining. *Compos Part Appl Sci Manuf* 39(6):923–929. <https://doi.org/10.1016/j.compositesa.2008.04.001>
- Wang Y, Zhang Z, Zhang G, Wang B, Zhang W (2018) Study on immersion waterjet assisted laser micromachining process. *J Mater Process Technol* 262:290–298. <https://doi.org/10.1016/j.jmatprotec.2018.07.004>
- Sala G (2000) Composite degradation due to fluid absorption. *Compos Part B Eng* 31:357–373. [https://doi.org/10.1016/S1359-8368\(00\)00025-1](https://doi.org/10.1016/S1359-8368(00)00025-1)
- Li M, Li S, Yang X, Zhang Y, Liang Z (2018) Fiber laser cutting of CFRP laminates with single- and multi-pass strategy: a feasibility study. *Opt Laser Technol* 107:443–453. <https://doi.org/10.1016/j.optlastec.2018.06.025>
- Li H, Ye Y, Du T, Zhao Y, Ren X, Hua Y (2022) The effect of thermal damage on mechanical strengths of CFRP cut with different pulse-width lasers. *Opt Laser Technol* 153:108219. <https://doi.org/10.1016/j.optlastec.2022.108219>
- Weber R, Hafner M, Michalowski A, Graf T (2011) Minimum damage in CFRP Laser Processing. *Phys Procedia* 12:302–307. <https://doi.org/10.1016/j.phpro.2011.03.137>
- Herzog D, Jaeschke P, Meier O, Haferkamp H (2008) Investigations on the thermal effect caused by laser cutting with respect to static strength of CFRP. *Int J Mach Tool Manu* 48(12–13):1464–1473. <https://doi.org/10.1016/j.ijmactools.2008.04.007>
- Li M, Li S, Gan G, Zhang Y, Liang Z, Yang X (2019) Experimental study on hole quality and tensile progressive failure following fiber laser cutting of multidirectional carbon fiber reinforced plastic laminates. *J Laser Appl* 31(1):012004. <https://doi.org/10.2351/1.5046549>
- Ramanujam N, Dhanabalan S, Raj Kumar D, Jeyaprakash N (2021) Investigation of Micro-hole Quality in Drilled CFRP laminates through CO<sub>2</sub> laser. *Arab J Sci Eng* 46(8):7557–7575. <https://doi.org/10.1007/s13369-021-05505-x>
- Zhou L, Zhou J, Huang P, Zhang G, Lin Z, Zhao Z, Huang Y, Jiao H, Long Y (2022) Study on the mechanism of quasi-continuous wave (QCW) fiber laser low-damage processing of carbon fiber-reinforced plastics. *Int J Adv Manuf Technol* 124(1–2):429–447. <https://doi.org/10.1007/s00170-022-10374-1>
- Sato Y, Tsukamoto M, Matsuoka F, Ohkubo T, Abe N (2017) Thermal effect on CFRP ablation with a 100-W class pulse fiber laser using a PCF amplifier. *Appl Surf Sci* 417:250–255. <https://doi.org/10.1016/j.apsusc.2017.03.286>
- Romoli L, Fischer F, Kling R (2012) A study on UV laser drilling of PEEK reinforced with carbon fibers. *Opt Lasers Eng* 50(3):449–457. <https://doi.org/10.1016/j.optlaseng.2011.10.008>
- Takahashi K, Tsukamoto M, Masuno S, Sato Y (2016) Heat conduction analysis of laser CFRP processing with IR and UV laser light. *Compos Part Appl Sci Manuf* 84:114–122. <https://doi.org/10.1016/j.compositesa.2015.12.009>
- Tao N, Chen G, Fang W, Li M (2023) Understanding the bowl-bottom effect in ultra-short pulsed laser drilling of CFRP laminate. *Compos Struct* 305:116498. <https://doi.org/10.1016/j.compstruct.2022.116498>
- Zhang H, Di J, Zhou M, Yan Y, Wang R (2015) An investigation on the hole quality during picosecond laser helical drilling of stainless steel 304. *Appl Phys A* 119(2):745–752. <https://doi.org/10.1007/s00339-015-9023-5>
- Kaspar J, Luft A, Nolte S, Will M, Beyer E (2006) Laser helical drilling of silicon wafers with ns to fs pulses: scanning electron microscopy and transmission electron microscopy characterization of drilled through-holes. *J Laser Appl* 18(2):85–92. <https://doi.org/10.2351/1.2164480>
- Li W, Huang Y, Chen X, Zhang G, Rong Y, Lu Y (2021) Study on laser drilling induced defects of CFRP plates with different scanning modes based on multi-pass strategy. *Opt Laser Technol* 144:107400. <https://doi.org/10.1016/j.optlastec.2021.107400>
- Wang L, Zhao W, Mei X, Yang Z, Shen X, Liu H (2020) Improving quality and machining efficiency of hole during AlN prepanning with nanosecond pulse laser. *Ceram Int* 46(15):24018–24028. <https://doi.org/10.1016/j.ceramint.2020.06.179>
- Li W, Zhang G, Huang Y, Rong Y (2021) UV laser high-quality drilling of CFRP plate with a new interlaced scanning mode. *Compos Struct* 273:114258. <https://doi.org/10.1016/j.compstruct.2021.114258>
- Chen L, Huang Y, Li W, Yang R, Chen X, Zhang G, Rong Y (2023) Acoustic emission monitoring and heat-affected zone evaluation of CFRP laser cutting. *Compos Struct* 304:116419. <https://doi.org/10.1016/j.compstruct.2022.116419>
- Wang P, Zhang Z, Liu D, Qiu W, Zhang Y, Zhang G (2022) Comparative investigations on machinability and surface integrity of CFRP plate by picosecond laser vs laser induced plasma micro-drilling. *Opt Laser Technol* 151:108022. <https://doi.org/10.1016/j.optlastec.2022.108022>
- Negarestani R, Li L, Sezer HK, Whitehead D, Methven J (2009) Nano-second pulsed DPSS nd:YAG laser cutting of CFRP composites with mixed reactive and inert gases. *Int J Adv Manuf Technol* 49(5–8):553–566. <https://doi.org/10.1007/s00170-009-2431-y>

32. Oh S, Lee I, Park Y-B, Ki H (2019) Investigation of cut quality in fiber laser cutting of CFRP. *Opt Laser Technol* 113:129–140. <https://doi.org/10.1016/j.optlastec.2018.12.018>

**Publisher's Note** Springer Nature remains neutral with regard to jurisdictional claims in published maps and institutional affiliations.

Springer Nature or its licensor (e.g. a society or other partner) holds exclusive rights to this article under a publishing agreement with the author(s) or other rightsholder(s); author self-archiving of the accepted manuscript version of this article is solely governed by the terms of such publishing agreement and applicable law.